Domain Structures and Roles in Bacteriophage HK97 Capsid Assembly and Maturation†

James M. Benevides,‡ Priya Bondre,‡ Robert L. Duda,§ Roger W. Hendrix,§ and George J. Thomas, Jr.*,‡

Division of Cell Biology and Biophysics, School of Biological Sciences, University of Missouri-Kansas City, Kansas City, Missouri 64110, and Pittsburgh Bacteriophage Institute and Department of Biological Sciences, University of Pittsburgh, Pittsburgh, Pennsylvania 15260

Received November 30, 2003; Revised Manuscript Received March 10, 2004

ABSTRACT: Head assembly in the double-stranded DNA coliphage HK97 involves initially the formation of the precursor shell Prohead I from ∼420 copies of a 384-residue subunit. This is followed by proteolytic removal of residues 2−103 to create Prohead II, and then reorganization and expansion of the shell lattice and covalent cross-linking of subunits make Head II. Here, we report and structurally interpret solution Raman spectra of Prohead I, Prohead II, and Head II particles. The Raman signatures of Prohead I and Prohead II indicate a common α/β fold for residues 104−385, and a strongly conserved tertiary structure. The Raman difference spectrum between Prohead I and Prohead II demonstrates that the N-terminal residues 2−103 (Δ-domain) form a predominantly α-helical fold devoid of β-strand. The conformation of the Δ-domain in Prohead I thus resembles that of the previously characterized scaffolding proteins of *Salmonella* phage P22 and *Bacillus* phage φ29 and suggests an analogous architectural role in mediating the assembly of a properly dimensioned precursor shell. The Prohead II → Head II transition is accompanied by significant reordering of both the secondary and tertiary structures of 104−385, wherein a large increase occurs in the percentage of β-strand (from 38 to 45%), and a marginal increase is observed in the percentage of α-helix (from 27 to 31%). Both are at the expense of unordered chain segments. Residue environments affected by HK97 shell maturation include the unique cysteine (Cys 362) and numerous tyrosines and tryptophans. The tertiary structural reorganization is reminiscent of that observed for the procapsid → capsid transformation of P22. The Raman signatures of aqueous and crystalline Head II reveal no significant differences between the crystal and solution structures.

The double-stranded (ds)[1] DNA bacteriophage HK97, which shares both host range and morphology with the well-known coliphage λ, provides an advantageous system for investigating the structural basis of protein self-assembly and viral capsid maturation (*1*). The initial steps in assembly of the isometric phage head of HK97 involve the formation of pentameric and hexameric capsomers from a 384-residue subunit (gp5, 42 kDa) and co-assembly of the capsomers into a precursor shell of 420 subunits (Prohead I). The N-terminal 102 residues of each Prohead I subunit are then proteolytically removed to produce Prohead II. This is followed by shell expansion through a series of intermediate structures and intersubunit cross-linking of the icosahedral lattice to finally yield the mature form of the shell, Head II (*1*). The pathway of HK97 head maturation is depicted schematically in Figure 1.

The cleavage of Prohead I subunits is catalyzed by a virally encoded protease that is packaged within the Prohead I shell. Image reconstructions of Prohead I and Prohead II developed from the data of electron cryomicroscopy (cryo-EM) show that, although the outer surfaces of the two particles are nearly the same, the shell interior and cross-section are extensively changed upon excision of residues 2−103 (previously defined as the Δ-domain) (*2*). Conformational properties of the excised Δ-domain and the extent to which its excision alters the secondary and tertiary structures of residues 104−385 have not been ascertained. The Δ-domain of gp5 has been proposed as the HK97 functional equivalent of a scaffolding protein, by analogy with the scaffolding that assists shell assembly in other dsDNA viruses (*1*). For example, the well-characterized 36-kDa scaffolding protein of *Salmonella* bacteriophage P22 ensures efficient construction of a properly dimensioned $T = 7$ icosahedral particle, yet is not a component of the mature virion (*3*−*7*). A similar function is fulfilled by the 11-kDa scaffolding protein of *Bacillus* phage φ29, for which the crystal structure has been determined recently (*8*). Like the P22 scaffolding protein, the HK97 Δ-domain is expelled from the precursor shell and is not required for subsequent maturation and DNA packaging events (*9*).

The transition of Prohead II to Head II occurs in vivo at the time of packaging the viral genome. A corresponding transition can be induced in vitro by lowering the solution pH or by other chemical treatments (*1*, *2*). The prohead-to-head transformation involves a large-scale reorganization of

† Support of this research by the National Institutes of Health (GM50776 and GM47795) is gratefully acknowledged.

* To whom correspondence should be addressed. Tel: 816-235-5247. Fax: 816-235-1503. E-mail: thomasgj@umkc.edu.

‡ University of Missouri-Kansas City.

§ University of Pittsburgh.

[1] Abbreviations: ds, double stranded; cryo-EM, electron cryomicroscopy; Tris, tris(hydroxymethyl)aminomethane; ML, mother liquor.

10.1021/bi0302494 CCC: $27.50
Published on Web 04/16/2004

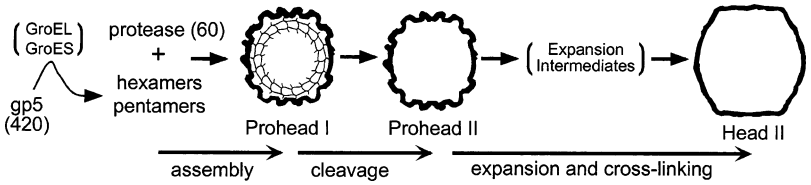

FIGURE 1: Assembly and maturation of the bacteriophage HK97 head shells, based on a variety of in vivo and in vitro observations. The dark outlines for Prohead I, Prohead II, and Head II are central sections of the respective shell structures determined by cryo-EM. Prohead I (left) is self-assembled from recombinantly produced gp5 (major capsid protein) in the absence of gp4 (protease). Prohead II is derived similarly, but from cells coexpressing both gp5 and gp4, which ensures cleavage of the N-terminal Δ-domain (residues 2−103). Head II is generated from Prohead II in vitro by low pH treatment followed by neutralization. This transition includes a substantial rearrangement of the subunit positions and conformations and the formation of 420 covalent cross-links. Further details of particle isolation, purification, and morphological characterization have been given elsewhere (*2*, *16*).

the subunit lattice, a substantial increase in particle diameter (from ∼450 to ∼650 Å), a dramatic decrease in shell thickness (from ∼50 to ∼18 Å), and localized refolding of subunit domains (*10*, *11*). Maturation to Head II is accompanied by formation of a network of intersubunit covalent bonds. The intersubunit cross-link consists of a novel isodipeptide bond between neighboring Lys 169 (N^{ζ}) and Asn 356 (C^{γ}) side chains (*2*). X-ray crystallography and cryo-EM provide details of subunit domain movements that occur during the Prohead II → Head II transformation in vitro and suggest a plausible molecular pathway via expansion intermediates (Figure 1) for in vivo HK97 head maturation (*10*−*12*).

Although the mature HK97 shell has been well characterized by high-resolution structural methods, specific mechanistic steps preceding Prohead II formation remain largely unresolved. In particular, the structure of the subunit Δ-domain within Prohead I is not known. Here, we employ Raman spectroscopy to investigate these questions. Solution Raman signatures of the Prohead I, Prohead II, and Head II particles have been obtained and compared with one another by digital difference methods. The Raman data are interpreted to reveal novel structural features of the subunits in Prohead I, Prohead II, and Head II assemblies, including the conformation of the subunit Δ-domain within Prohead I.

In previous work, Raman spectroscopy has been employed to investigate both structural and dynamic properties of the precursor shell (procapsid) and mature shell (capsid) of bacteriophage P22 (*4*, *5*, *13*−*15*). The P22 studies constitute a baseline for Raman analysis of the structures and interactions of scaffolding and shell subunits within the context of icosahedral capsid maturation. The present findings on HK97 are discussed in relation to those obtained on the P22 system. Finally, we compare the solution Raman results on HK97 with preliminary Raman data obtained from the Head II crystal characterized by X-ray crystallography (*10*).

MATERIALS AND METHODS

1. Sample Preparations. (a) Proheads. HK97 Prohead I and Prohead II were made by expressing HK97 proteins from plasmids pT7−5Hd2.9 and pT7−5Hd2.9(*fsBstBI*) and were purified initially by a combination of differential centrifugation, polyethlyene glycol precipitation, and velocity sedimentation in glycerol gradients, essentially as described by Duda et al. (*16*). Prohead I and Prohead II were further purified by adsorption to a column of Whatman DE-52 in 20 mM tris(hydroxymethyl)aminomethane hydrochloride (Tris HCl) pH 7.5 with 40 mM NaCl, and elution with a linear gradient of NaCl (to 0.3 M). All final preparations were concentrated by centrifugation, ultracentrifugation, and resuspension in a small volume of buffer for further studies.

(b) Head II. Prohead II, as purified above, was converted to Head II in a two-step procedure. To induce expansion, Prohead II samples (in 20 mM Tris HCl, pH 7.5, 0.2 M KCl, 1 mM 2-mercaptoethanol) were diluted about 5-fold into acidic urea at a final concentration of 7 M urea in 50 mM sodium acetate, pH 5. After 60 min, the samples were diluted 5-fold in 50 mM Tris HCl, pH 7.5 and dialyzed exhaustively in the cold to remove urea.

2. Raman Spectroscopy. HK97 Prohead I (40 mg/mL), Prohead II (40 mg/mL), and Head II (46 mg/mL), each in 20 mM Tris, 100 mM KCl, 1 mM β-mercaptoethanol, pH 7.5 ± 0.1 solution, were sealed in glass capillary cells (Kimax 34502) and thermostated at 20 °C for Raman spectroscopy. The Raman spectra were excited at 532 nm using a NdY: VO_4 diode laser (model Verdi 5W, Coherent, Santa Clara, CA) with 100 mW of radiant power at the sample. A holographic band-pass filter (Kaiser Optical, Ann Arbor, MI) was employed to reject Rayleigh scattering. The Raman scattering in the spectral regions 600−1800 cm^{-1} and 2300−2800 cm^{-1} were collected using a single-grating spectrograph (model Spex 500M, ISA, Edison, NJ) equipped with a back-thinned liquid nitrogen cooled charge-coupled-device detector (Spectrum One, ISA, Edison, NJ). A detailed description of this instrumentation has been given elsewhere (*17*). The Raman spectra of the 500−1800 cm^{-1} interval represent averages of seven cycles of data collection, each consisting of seven independent accumulations of 40 s duration. The Raman spectra of the 2300−2800 cm^{-1} interval involved averaging of 36 cycles of 20 accumulations, each of 40 s duration. The Raman frequencies (wavenumbers) of sharp or intense bands are accurate to ±1.0 cm^{-1}; those of weak, broad or overlapping bands are accurate to ±2.0 cm^{-1}. The spectral resolution is 4 cm^{-1} or better.

Single crystals of Head II, which were suspended in the same mother liquor (ML) employed for X-ray diffraction analysis (*10*), were mounted in glass capillaries for examination using the spectrometer described above. Mineral oil was positioned on either side of the ML, and the capillary ends were occluded with sealing wax. In each experimental protocol, Raman spectra were collected from both the single crystal and ML. The position of the glass capillary in the sample chamber was adjusted to obtain optimal Raman scattering from the crystal or ML. Raman bands of the ML that contributed to the spectral trace of the crystal were removed by appropriate spectral subtraction (*18*).

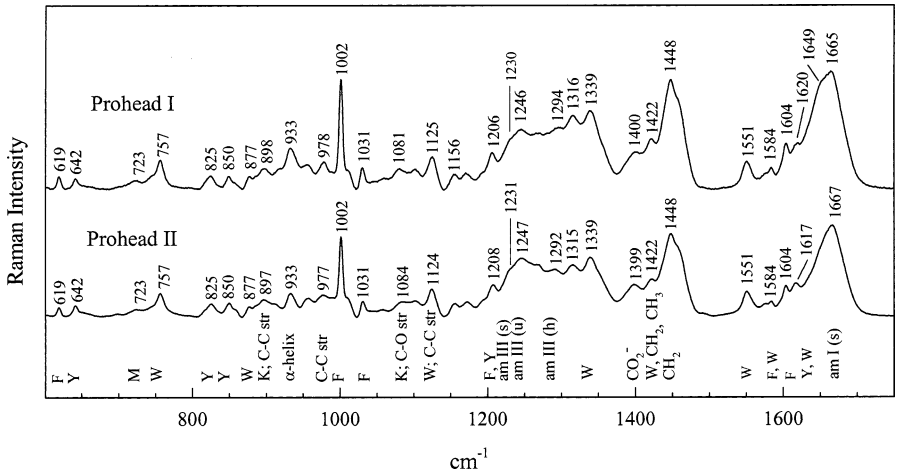

FIGURE 2: Raman spectra (600−1800 cm^{-1}) of the HK97 Prohead I (top) and Prohead II (bottom) particles, each at ~40 mg/mL in 20 mM Tris, pH 7.5 solution containing 100 mM KCl and 1 mM β-mercaptoethanol. Although the ordinate is arbitrary, the two spectra have been scaled to produce identical intensities for their respective tyrosine Raman markers at 642 cm^{-1}. The 642 cm^{-1} intensity is invariant to the tyrosine environment (*26*). The N-terminal sequence (2−103) cleaved from the Prohead I subunit contains no tyrosines. Numerical labels indicate wavenumber values (cm^{-1}) for prominent Raman bands for which residue and chemical group assignments are indicated along the abscissa. Additional assignments are given in Table 1.

RESULTS AND INTERPRETATION

1. Raman Spectroscopy of Prohead I and Prohead II. (a) Subunit Secondary Structures of Prohead I and Prohead II. Figure 2 compares Raman spectra of Prohead I (top trace) and Prohead II (bottom trace) in the region 600−1800 cm^{-1}. Specific Raman band assignments are given in Table 1. The Raman signature of Prohead I is dominated by an intense and broad amide I band with principal peak at 1665 cm^{-1}, which is diagnostic of nonhelical secondary structure, and a prominent shoulder at 1649 cm^{-1}, which is indicative of α-helix (*19*−*22*). The prominent α-helix marker (1649 cm^{-1}) of Prohead I is significantly attenuated in Prohead II. Different secondary structure distributions for Prohead I and Prohead II subunits are also apparent from the Raman band profiles within the amide III region (1220−1350 cm^{-1}). Thus, amide III markers of α-helix, which are expected in the interval 1275−1320 cm^{-1} (*20*, *22*), are more prominent for the Prohead I spectrum than for the Prohead II spectrum. Another reliable Raman indicator of α-helical secondary structure, the band at 933 cm^{-1} (*23*, *24*), is about 2-fold more intense in the spectrum of Prohead I than in that of Prohead II.

Use of the reference intensity profile method (*25*) to fit the observed Raman amide I bands of Prohead I and Prohead II provides a quantitative estimate of the subunit secondary structure distribution in each particle. The results of this analysis are summarized in Table 2. It is clear that truncation of the N-terminal residues 2−103 from the Prohead I subunit greatly diminishes the α-helical content of the protein (reduced from 40 to 27%), whereas the percentages of β-strand and irregular conformations are much less affected.

(b) Secondary Structure of the Δ-Domain. The Raman signature of the Δ-domain, which is generated by subtracting the Raman spectrum of Prohead II from that of Prohead I, is shown in Figure 3 (bottom trace) and indicates a predominantly α-helical secondary structure for the Δ-domain of the Prohead I subunit. For this spectral subtraction, we have employed as the intensity standard the 642 cm^{-1} marker of tyrosine, which is insensitive to changes in either secondary or tertiary structure (*26*). Use of the 642 cm^{-1} band as the normalization standard is also favored by the absence of tyrosine from the Δ-domain. The computed Raman signature of the Δ-domain exhibits all of the secondary structure markers expected of a protein domain consisting primarily of α-helices and interconnecting irregular chain conformations, but lacking appreciable β-strand. Application of the reference intensity profile (*25*) method to the computed Raman amide I profile of the Δ-domain also provides a quantitative assessment of the secondary structure distribution, as given in Table 2. The richness of α-helix (74%) and the deficiency of β-strand (10%) in the Δ-domain structure demonstrate further that the α-helices, if short, are interconnected primarily by turns, loops, or unordered chain segments consisting of at most a few residues each. Alternatively, the nonhelical segments may occur at the ends of an extended α-helix. A similar secondary structure distribution has been proposed for the scaffolding protein of bacteriophage P22, based upon analysis of its Raman spectrum (*4*). The Raman spectrum of the P22 scaffolding protein is included in Figure 3 (top trace) for comparison with the computed spectrum of the HK97 Δ-domain.

It is noteworthy that the Prohead I-minus-Prohead II difference spectrum (Figure 3, bottom trace) reveals no derivative-type features. This indicates that local environments of the numerous side chains contributing to the Raman spectra of the prohead particles (see assignments of Table 1) are essentially unaltered by Δ-domain elimination. Accordingly, we conclude that the tertiary fold of residues 104−385 in the full-length subunit of Prohead I is largely conserved in the truncated subunit of Prohead II. Such conservation of tertiary structure supports the assumption, which is implicit in the above spectral subtraction procedure and difference data analysis, that the secondary structure of the 104−385 core of gp5 is essentially invariant to cleavage of the Δ-domain.

(c) Local Side-Chain Environments. (1) Tyrosine. The seven tyrosines of the gp5 subunit (Tyr 150, Tyr 206, Tyr 213, Tyr 243, Tyr 263, Tyr 295, Tyr 371) are located outside the Δ-domain. Each contributes to the pair of tyrosine marker

Table 1: Raman Frequencies, Intensities and Assignments for HK97 Prohead I, Prohead II, and Head II Empty Shells[a]

Prohead I		Prohead II		Head II		
cm^{-1}	I^b	cm^{-1}	I	cm^{-1}	I	assignments[c]
619	1.1	619	0.8	621	1.0	F
642	0.9	642	1.2	643	1.1	Y
649bs	0.4	649bs	0.4	649bs	0.4	
699	0.3	699	0.6	700b	0.6	amide V
723	0.8	723b	0.9	725	0.9	M, Y
745s	1.2	745s	1.4	748s	1.5	sc
757	2.5	757	2.9	757		W
825	1.1	825	1.4	828	1.0	Y
850	1.1	850	1.5	851	2.2	Y
857s	0.6	858s	0.9			
877	1.0	877	1.1	877	2.3	W
898	1.7	897	2.6	896	2.0	sc
916	2.5	912s	0.9	914	1.7	sc
933	3.5	933	1.8	933	2.3	α-helix [$\nu(C^{\alpha}-C^{\beta})$]
956	2.1	957	1.2	957	2.1	sc
978	2.3	977	1.8	976	1.9	sc
1002	9.3	1002	8.6	1002	8.2	F
1012s	1.6	1011s	2.0	1011	2.7	W
1031	1.8	1031	1.8	1032	1.4	F
1060	1.0	1058	0.9	1058	1.2	sc[ν(C−C,C−O)]
1081	1.7	1084b	1.6	1081	1.6	K, sc [ν(C−C,C−N,C−O)]
1102	1.7	1102	1.7	1099	1.9	sc[ν(C−C)]
1125	2.8	1124	2.9	1125	3.1	W, sc[ν(C−C)]
1156	1.3	1156	1.4	1154	1.4	$\delta(CH_3)$
1172	1.4	1173	1.6	1172	1.5	Y, $\delta(CH_3)$
1192	1.5	1193s	2.0	1197s	1.2	
1206	3.2	1208	3.7	1209	3.5	F, Y
1230	4.3	1231s	5.7	1231s	5.2	amide III (β-sheet)
1246	5.1	1247	6.7	1243	5.6	amide III (turns, coil)
1270	4.8	1270s	5.9	1271	5.1	amide III (α-helix)
1294	5.2	1292	5.4	1287	4.5	amide III (α-helix)
1316	6.3	1315	5.8	1316	5.3	$\delta(CH_2)$
1339	6.7	1339	6.7	1340	5.6	W
1357s	3.6			1354s	4.4	W
1400	3.2	1399	3.7	1399	2.9	D, E [$\nu(CO_2^-)$]
1422	4.4	1422	4.1	1424	3.7	W, $\delta(CH_2)$, $\delta(CH_3)$
1448	9.3	1448	8.9	1449	8.5	$\delta(CH_2)$
1460s	7.8	1458s	7.6	1458s	7.2	W
1551	2.4	1551	2.9	1555	2.7	W
1575	1.4	1575	1.4	1576s	1.0	F,W
1584	1.9	1584	1.6	1585	1.3	F, W
1604	3.8	1604	3.4	1604	3.1	F
1620	8.6	1617	3.7	1618	3.7	Y, W
1649	9.2			1657s	8.7	amide I (α-helix)
1665	10.0	1667	10.0	1667	10.0	amide I (β-strand)
2579	0.4	2573	0.4	2564	0.4	C [ν(S−H)]

[a] Wavenumbers (cm^{-1} units) and relative intensities (0−10 scale) are from Figures 2 and 5. [b] I = intensity. [c] Abbreviations: b, broad; s, shoulder; sc, side chain; ν, bond stretching; δ bond angle deformation.

bands at 850 and 825 cm^{-1}. The tyrosine doublet intensity ratio (I_{850}/I_{825}) is diagnostic of the hydrogen bonding state of the average phenoxyl group, as follows: $I_{850}/I_{825} = 0.3$, if O−H is a strong hydrogen-bond donor; $I_{850}/I_{825} = 2.5$, if O−H is a strong hydrogen-bond acceptor; $I_{850}/I_{825} = 1.25$, if O−H is both donor and acceptor (e.g., a solvent-exposed phenoxyl); and $I_{850}/I_{825} = 6.7$ if O−H is not hydrogen bonded (*27*, *28*). For globular proteins and their assemblies in solution, the last state is not ordinarily encountered (*28*) and the expected range for gp5 is therefore $0.3 < I_{850}/I_{825} < 2.5$. The data of Figure 2 indicate $I_{850}/I_{825} = 1.0 \pm 0.05$ for both the Prohead I and Prohead II particles, which signifies a modest excess of phenoxyl donors over acceptors in both assemblies. The data are consistent with solvent exposure

Table 2: Secondary Structures of HK97 Prohead I, Prohead II, and Head II Subunits Based upon Curve-Fitting of Raman Amide I Bands[a]

structure	Prohead I[b]	Δ-Domain[c]	Prohead II[d]	Head II[e,f]
α-helix	40 ± 4%	74 ± 5%	27 ± 3%	31 ± 3% (28%)
β-strand	31 ± 3%	10 ± 2%	38 ± 4%	45 ± 5% (32%)
irregular	29 ± 3%	16 ± 2%	35 ± 3%	24 ± 3% (40%)

[a] Method of Berjot et al., 1987 (*25*). [b] Prohead I (subunit residues 2−385) at 2 mM subunit concentration. [c] Prohead I (subunit residues 2−103, Figure 3, bottom) at 2 mM subunit concentration. For comparison, amide I of the P22 scaffolding protein at 2 mM concentration (Figure 3, top) indicates 75 ± 4% α-helix, 15 ± 2% β-strand and 10 ± 2% irregular structure. [d] Prohead II at 2 mM subunit concentration. [e] Head II at 2 mM subunit concentration. [f] Values in parentheses are based upon the X-ray crystal structure of Head II (*10*). (See also discussion in text.)

of most, if not all, tyrosine phenoxyls. Importantly, I_{850}/I_{825} is invariant to the Prohead I → Prohead II transition. This is consistent with the concept of conserved domain structures in the 104−385 sequence.

(2) Tryptophan. Several conformation- or interaction-sensitive Raman markers of the indolyl side chain of tryptophan have been identified (*29*−*32*). In Prohead I and Prohead II, these Raman markers, which are diagnostic of the average environment of residues Trp 89, Trp 189, Trp 282, Trp 309, and Trp 336, occcur near 880, 1340/1360, and 1551 cm^{-1} (Table 1). The present results indicate the following properties of the average tryptophan in both Prohead I and Prohead II: a value of 95° for the magnitude of the side-chain torsion angle ($|\chi^{2,1}|$) defined by $C^{\alpha}-C^{\beta}-C^{\gamma}-C^{\delta 1}$, moderate hydrogen bonding of the $N^{\epsilon}H$ donor site, and a hydrophilic indolyl ring environment. Because Trp 89 occurs within the Δ-domain, the tryptophan Raman markers are correspondingly less intense (∼20%) in Prohead II than in Prohead I. Nevertheless, the invariance of the band positions to Δ-domain cleavage demonstrates that the indoles do not interact differently in the full-length and truncated subunits, again consistent with conserved domain structure in the 104−385 sequence.

(3) Cysteine. The Raman marker of the cysteine sulfhydryl (S−H) moiety is diagnostic of the strength of S−H···X hydrogen bonding. Here, X represents an appropriate acceptor site of the protein (usually O or N) or solvent (O), and the Raman wavenumber value decreases with increasing hydrogen-bond strength (*33*). The unique cysteine residue (Cys 362) of gp5, which is situated near to the protein C-terminus, generates distinguishable Raman markers in Prohead I (2579 cm^{-1}) and Prohead II (2573 cm^{-1}) particles, as shown in Figure 4. These distinctive markers identify a sulfhydryl hydrogen-bond strength that is weak in Prohead I and slightly stronger in Prohead II (*22*, *33*, *34*). The computed difference spectrum of Figure 4 underscores the relatively small but clear-cut Raman S−H band shift to lower wavenumber value with the Prohead I → Prohead II transition. This finding demonstrates that the specific locus of the Cys 362 sulfhydryl bond is perturbed, albeit slightly, with Δ-domain cleavage.

2. Raman Spectroscopy of Head II. Figure 5 compares the Raman spectrum of Head II (top trace) with that of Prohead II (second-from-top trace) for the region 600−1800 cm^{-1}. Also shown is the difference spectrum computed between Head II and Prohead II (second-from-bottom trace) and a

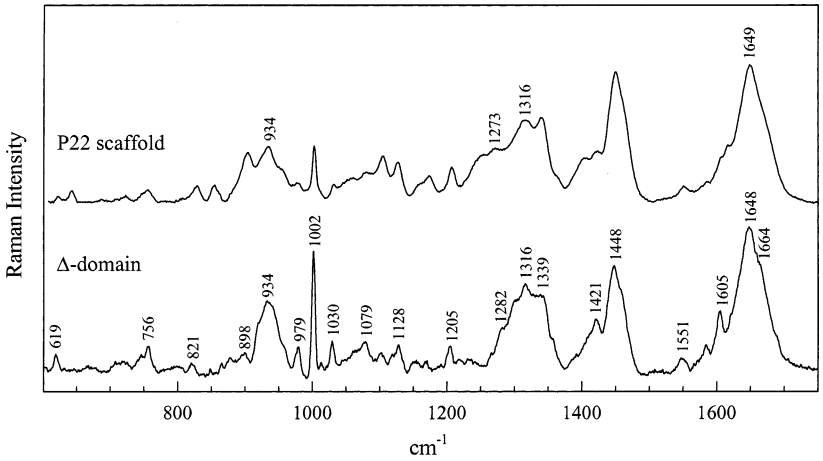

FIGURE 3: The Raman spectrum (600−1800 cm^{-1}) of the Δ-domain (bottom) obtained by subtracting the Raman spectrum of Prohead II from that of Prohead I. The ordinate scale is expanded 3-fold over that shown in Figure 2. Shown for comparison is the Raman spectrum of the P22 scaffolding protein (top), obtained at similar experimental conditions.

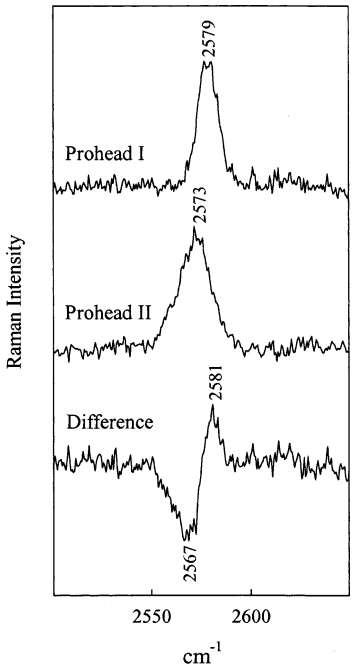

FIGURE 4: Raman sulfhydryl signatures of Cys 362 in Prohead I (top) and Prohead II (middle) particles and their computed difference spectrum (bottom). The ordinate is expanded approximately 10-fold over that shown in Figure 2. Other conditions are as given in Figure 2.

3-fold amplification of the difference (bottom trace). The difference profile is rich in peaks and troughs, and these are distributed throughout the spectrum, indicating major changes in subunit secondary and tertiary structures accompanying the Prohead II → Head II transition.

(a) Changes in Subunit Secondary Structure. The amide I difference peaks at 1654 and 1669 cm^{-1} in the Figure 5 difference spectrum are diagnostic of marginal and large increases, respectively, in subunit α-helix and β-strand structures in the Head II subunit vis-à-vis the Prohead II subunit. Amide III peaks below 1240 cm^{-1} and at 1275 and 1317 cm^{-1} are consistent with this conclusion. Enhancements of ordered conformations occur at the expense of turns and unordered conformations, as evidenced by the amide I troughs at 1683 and 1699 cm^{-1} and an amide III trough at 1258 cm^{-1}. The magnitudes of the amide I difference peaks and troughs in Figure 5 suggest a conversion of ∼10% of the subunit main chain from unordered to ordered conformations (predominantly β-strand) with the Prohead II → Head II transition.

(b) Changes in Side Chain Environments. (1) Tyrosine. In contrast to conserved tyrosine environments for the Prohead I → Prohead II transition, the average tyrosine phenoxyl hydrogen bonding state is dramatically changed with the Prohead II → Head II transformation. We find that I_{850}/I_{825} increases from 1.00 ± 0.05 to 2.00 ± 0.05 with head maturation. The majority of tyrosines in the Head II subunit become acceptors of strong hydrogen bonds from robust donors.

(2) Tryptophan. Tryptophans of Head II, by virtue of a distinctive Raman marker at 1555 cm^{-1} and altered intensities in the 1340/1360 cm^{-1} doublet, are also greatly differentiated from those of Prohead II and Prohead I (cf. Figures 2 and 5). The data indicate for tryptophans of Head II that the magnitude of the average $\chi^{2,1}$ torsion is 104°, compared to 95° for proheads, and that the average hydrophobicity of the indolyl ring environment has increased markedly. These changes are consistent with burying of Trp side chains.

(3) Cysteine. The cysteine S−H marker of Prohead II (2573 cm^{-1}) is shifted to 2564 cm^{-1} in Head II (Figure 6), indicating a substantial increase in the strength of S−H···X hydrogen bonding.

(4) Aspartate and Glutamate. The trough at 1404 cm^{-1} in the Figure 5 difference spectrum is attributed to diminished intensity in Head II of the Raman marker (1399 cm^{-1}) of ionized carboxylate moieties (CO_2^-) as compared with Prohead II. This implies a stable subpopulation of protonated carboxyls (CO_2H) among the 34 acidic side chains per subunit (19 Asp + 15 Glu). It should be noted that, although the Head II transformation is triggered by lowering the pH of the Prohead II solution to pH 4, the product is restored to pH 7.5 following the irreversible shell tansformation, and thus all samples investigated here were examined at pH 7.5. Ordinarily, we anticipate for CO_2^- → CO_2H protonation an enhancement of Raman intensity near 1700 cm^{-1} (*35*); yet, no candidate peak is observed in the Figure 5 difference spectrum. However, the expected CO_2H marker is intrinsically weak and may simply be obscured by the overlapping amide features occurring just below 1700 cm^{-1}. If the

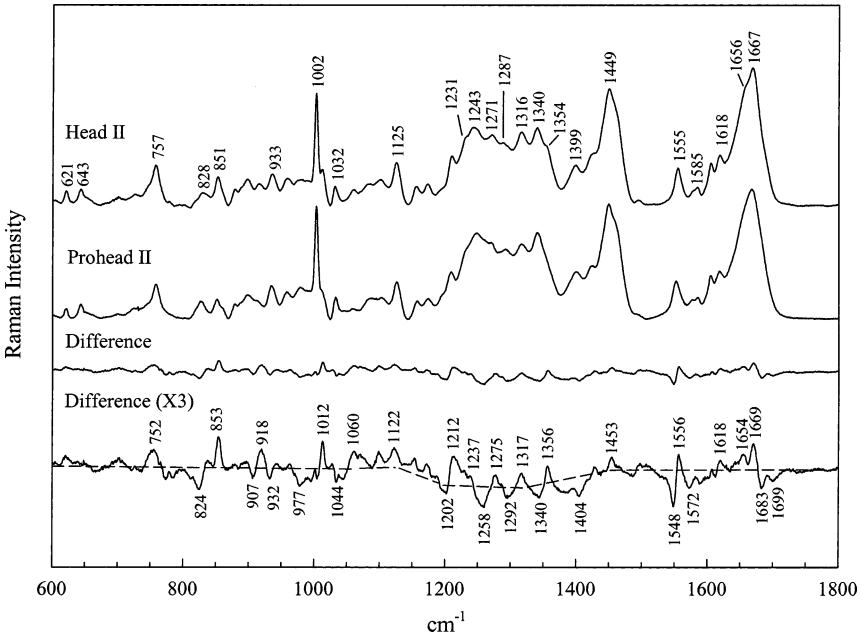

FIGURE 5: Raman spectra (600−1800 cm^{-1}) of the HK97 Head II (top) and Prohead II (second-from-top) particles, normalized to the intensity of the 1449 cm^{-1} peak. The computed difference spectrum (second-from-bottom) and 3-fold amplification of the difference (bottom) are also shown. Other conditions are as given in Figure 2.

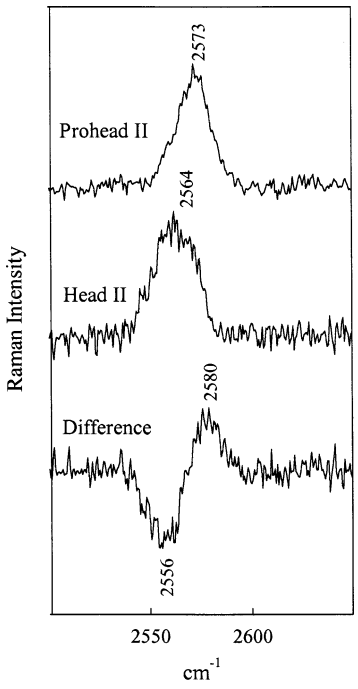

FIGURE 6: Raman sulfhydryl signatures of Cys 362 in Prohead II (top) and Head II (middle) particles and their computed difference spectrum (bottom). The ordinate is expanded approximately 10-fold over that shown in Figure 5. Other conditions are as given in Figure 2.

population of ionized carboxylates is lower in Head II than in Prohead II, notwithstanding the identical pH values of their solutions, then specific protonated carboxyls may be essential for stabilization of the mature head. Comparison of the data of Figure 5 with model compound studies (*35*) suggests that roughly 5−10% of the subunit carboxylates (2−4 residues) are protonated in the Head II assembly.

(5) Other Side Chains. The large number of additional peaks and troughs distributed throughout the Figure 5 difference spectrum represent altered local environments and interactions of diverse side chains. In some cases, the particular moieties affected can be determined from the assignments given in Table 1. The extent of these perturbations confirms that the tertiary structure of the 104−385 subunit undergoes a global reorganization with shell expansion and catenation.

(c) Spectral Evidence of the Lys 169−Asn 356 Linkage. The isodipeptide bonds, which catenate the Head II lattice by linking the N^{ζ} site of Lys 169 in each subunit with the C^{γ} site of Asn 356 in a neighboring subunit, are expected to contribute only feebly to the Raman spectrum. Previous studies indicate that the lysyl $C^{\gamma}-N^{\zeta}$ bond contributes to Raman markers near 890, 935, 965, 1055, and 1070 cm^{-1} (*36*). The isodipeptide bond could perturb one or more of these lysyl Raman markers. Accordingly, the troughs at 932, 977, and 1044 cm^{-1} and the peaks at 918 and 1060 cm^{-1} in the Figure 5 difference spectrum are plausible Raman markers of the catenated capsid. Similarly, because the linkage of lysyl N^{ζ} to C^{γ} modifies the adjoining bond of the asparagyl C═O group, a small spectral perturbation could also occur in the carbonyl region (1650−1750 cm^{-1}). This may contribute to the very weak difference peak near 1720 cm^{-1} and companion trough near 1699 cm^{-1} (Figure 5). Further studies of model compounds will be required to reach more definitive assignments.

3. Comparison of the Raman Signatures of Head II in Solution and Crystal States. Figure 7 compares the solution Raman signature of Head II (trace D) with that of a single-crystal suspended in ML (trace A). Subtraction of the ML (trace B) and appropriate amplification of the difference gives the signature of the Head II crystal (trace C). Although the quality of the crystal spectrum obtained by difference is inferior to that of the solution (owing to lower protein density for the ML-suspended crystal vis-à-vis the solution, and to interfering Raman bands of the ML), Figure 7 demonstrates nevertheless a close correspondence between the Head II structure in the solution and crystal states. Notably, the

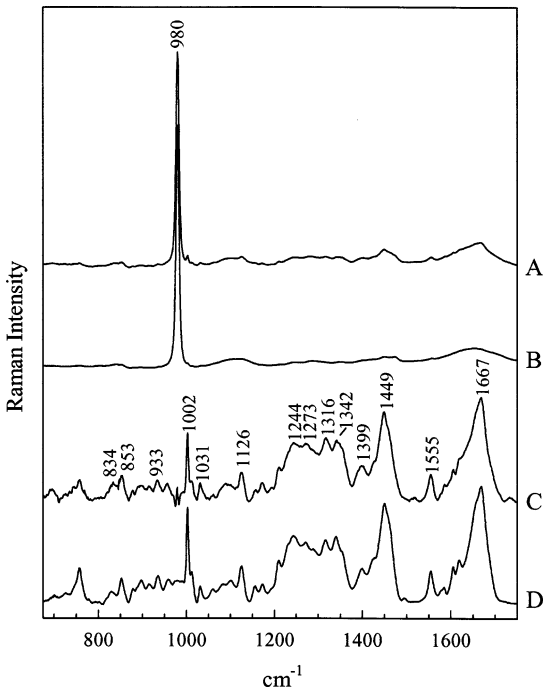

FIGURE 7: Raman spectra in the region 675−1750 cm^{-1} of a single crystal of Head II in mother liquor (trace A) and of pure mother liquor (trace B), each normalized to the intensity of the phosphate marker at 980 cm^{-1}. Subtraction of the two (A − B) and 10-fold amplification yields trace C, which represents the Raman signature of the Head II crystal. For comparison, trace D shows the Raman spectrum of the Head II solution (from Figure 5).

identical amide I peaks (1667 cm^{-1}) and comparable amide III profiles (shoulder at 1231 cm^{-1}, and maxima at 1244 and 1273 cm^{-1}) confirm the same subunit secondary structures. The patterns of side-chain markers are also very similar for solution and crystal forms of Head II.

DISCUSSION AND CONCLUSIONS

Raman spectra of bacteriophage HK97 Prohead I and Prohead II reveal that the surface lattices of both consist of a structurally conserved subunit domain (residues 104−385). The results suggest that this conserved structure (α/β conformation, Table 2) may function in vivo as a subunit core or "platform" upon which the Δ-domain is poised in Prohead I for removal by action of the virally encoded protease, gp4. The secondary structure of the subunit Δ-domain within the context of the Prohead I lattice was not determined in previous studies of HK97 shells (*10*, *11*) but has been addressed here by difference Raman methods. Raman analysis shows that the Δ-domain is predominantly α-helical (74%), deficient in β-strand (10%) and consisting of a modest proportion of unordered or irregular main-chain structure (16%). Accordingly, the Δ-domain appears to exhibit architectural similarities to the well-characterized scaffolding protein subunit (gp8) of the dsDNA bacteriophage P22 (*4*, *5*). These conclusions agree with earlier predictions of the secondary structure of the Δ-domain based on the amino acid sequence (*2*).

The conformational similarities of the Δ-domain and the P22 scaffolding subunit and their analogous removal from the procapsid after initial assembly support the notion that the Δ-domain fulfills a scaffolding-like role in HK97 shell assembly (*2*). In accordance with this role, we believe that the Δ-domain may project from the α/β platform toward the interior of the prohead shell as proposed by Conway et al. (*2*, *11*), either as an extended helix that is connected to the platform by a flexible chain segment or as a collection of shorter helices interconnected by numerous flexible links (turns, loops, and/or coils) (Figure 8). In an extension of this model, the Δ-domains in Prohead I could serve to occupy much of the shell interior and effectively occlude host proteases, nucleases or other cellular agents that might be refractive to progression along the native phage assembly pathway.

Interestingly, the Δ-domain contains a high proportion of ionized residues (31%) and a low net charge (4 Asp, 13 Glu, 13 Lys, 2 Arg). These attributes may facilitate electrostatic interactions favorable to helix packing within the shell interior and solubilization of the products of Δ-domain proteolysis.

In contrast to the conservation of the structure of the gp5 core (104−385) with the Prohead I → Prohead II transition, significant reordering of secondary structure and extensive changes in tertiary structure accompany the maturation of Prohead II to Head II. We observe a relatively large increase in β-strand (7%) and a marginal increase in α-helix (4%) at the expense of unordered chain segments (Table 2), and altered Raman markers of many side chains (Table 1). Similar structural changes occur with the subunit reorganizations in P22 (*14*, *37*) and PRD1 shells (*38*). However, unlike P22 and PRD1 capsid subunits, which are highly β-stranded, the Head II subunit of HK97 is highly α-helical.

The Raman spectrum of Head II provides convincing evidence of a much higher proportion of subunit α-helix structure (31%) than is present in subunits of either P22 (15%) or PRD1 (18%) (*15*, *38*). This is consistent with the Head II X-ray structure, which reveals mixed α/β domains (A and P), and two potentially flexible extensions, the N-arm, and an antiparallel β-strand hairpin, the E-loop. Cryo-EM reconstructions suggest that the N-arm and E-loop undergo refolding with the Prohead II → Head II transition (*10*, *11*). The increases in secondary structure observed by Raman spectroscopy to accompany the Prohead II → Head II transition presumably involve refolding of the flexible extensions and lead to a net increase primarily in β-strand content. We note, however, that the Raman amide I curve fitting method employed here (*25*) suggests a Head II subunit β-strand content (45 ± 5%) that is somewhat higher than the average computed from X-ray coordinates (*10*) (Table 2). This may reflect different proportions of β-strand in subunits of the solution and crystal structures of Head II. However, such discordance between Raman and X-ray results can more likely be attributed to the fact that the Raman amide I band serves specifically as a marker of the local Ramachandran angles (φ,ψ) of the peptide residues rather than of the global fold in which the residues occur (*20*, *21*, *39*).

Changes in the environments of side chains with the Prohead II → Head II transition are not revealed in X-ray and cryo-EM based models (*10*, *11*). The Raman spectra, however, identify many of the side chains suffering altered local interactions with maturation (Table 1). These interactions, which occur both within and between Head II capsomers, presumably stabilize Head II relative to Prohead II enabling the shell to withstand the forces generated during DNA packaging. The present results show that tyrosines (Tyr

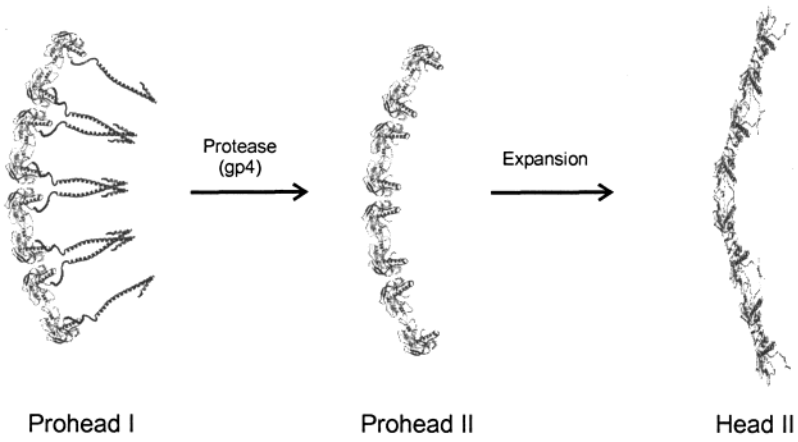

FIGURE 8: A plausible scheme for Δ-domain participation in HK97 Prohead maturation. The 75% α-helical Δ-domain (residues 2−103), which is involved in intersubunit recognition during early stages of shell assembly (*1*, *2*, *9*), is modeled here by analogy with the similarly helical scaffolding protein of phage φ29 (*8*) and is proposed as projecting toward the interior of the Prohead II shell (left) to facilitate occlusion of unwanted molecular material from the cavity. Neither the lengths and distributions of the helical modules nor the actual 3D structure of the Δ-domain are known. Residues 104−385, which form an α/β platform for the Δ-domain of the Prohead I subunit and are structurally invariant to the protease-induced Prohead I → Prohead II transition (center), undergo large changes in secondary and tertiary structures with maturation to the Head II shell (right).

150, Tyr 206, Tyr 213, Tyr 243, Tyr 263, Tyr 295, Tyr 371), tryptophans (Trp 189, Trp 282, Trp 309, Trp 336) and the single cysteine (Cys 362) of the 104−385 subunit fulfill key roles in this lattice stabilization. Consistent with these results, Raman experiments monitoring deuterium exchange protection show that the Trp residues are significantly more protected in Head II than in Prohead II (unpublished results).

Raman spectroscopy has been employed to characterize both structural and dynamic properties of P22 shell assemblies, including the precursor (procapsid) and mature (capsid) states of the phage head (*4*, *5*, *13*−*15*, *40*). It is of interest to compare the previous findings on P22 with current results on HK97. Assembly of a properly dimensioned P22 procapsid ($T = 7$) requires 200−300 copies of a scaffolding subunit (gp8, 34 kDa) in addition to 420 copies of major coat protein (gp5, 47 kDa). The P22 scaffolding subunit is highly α-helical, deficient in β-strand, devoid of the exchange-protected core usually present in globular proteins, and prone to oligomerization when the local subunit concentration is high (*5*, *7*, *15*, *40*). The P22 scaffolding subunit thus appears to consist of a loosely organized ensemble of α-helical domains, capable of occupying the procapsid interior as monomers, dimers, and higher order oligomers. In the case of HK97, although $T = 7$ shell assembly proceeds without the requirement of a scaffolding subunit, the Prohead I subunit contains the Δ-domain which has no counterpart in P22. The present analysis of Δ-domain secondary structure reveals the same high α-helicity previously detected for the P22 scaffolding subunit (*4*), in support of a similarity of function in mediating $T = 7$ shell construction (*2*, *16*). Consistent with this role, we expect the Δ-domain helices to be both flexible and conducive to intersubunit associations. Interconversion between long and short helical segments could provide an ideal dynamic to exclude cellular material from the nascent shell interior while retaining favorability as a substrate for proteolysis once shell assembly has been completed.

We have noted that the Raman signature of the Prohead I → Prohead II transition is characterized by highly conserved secondary and tertiary structures for residues 104−385 of the shell subunit platform, whereas large structural changes are observed with the Prohead II → Head II maturation. In contrast, the local structure in the vicinity of residue Cys 362 changes significantly for *both* shell transformations (cf. Figures 4 and 6). With the Prohead I → Prohead II transition, the Cys 362 sulfhydryl undergoes a change from weak to moderate hydrogen-bond donor, and with the Prohead II → Head II maturation, the strength of S−H···X interaction increases still further so that ultimately a robust hydrogen bond is formed (*33*). The acceptor atom (X), which is not identified in any of the Raman spectra, is likely to be the oxygen of a main-chain (amide) or side chain (carbonyl) site (*34*). In the X-ray structure of Head II, Cys 362 is located in the βJ-strand of the P domain. It appears to be in a largely hydrophobic pocket, most likely sequestered from solvent, but the disposition of the sulfhydryl moiety is not revealed (*10*), nor is Cys 362 located in cryo-EM reconstructions of the proheads (*11*). Although Cys 362 may well have a crucial role in the biological function of the protein, it appears unlikely that cysteine is the only amino acid that can fulfill such a role. The only mutation that has been made at this site, Cys 362 → Ser, is normal or nearly so in the various steps of assembly and maturation (*9*, *41*). We also note that two other phages, BFK20 (GenBank Accession No. AJ278322) and D3 (*42*), which contain amino acid sequences very similar to HK97 and hence are clearly related in structure, have Ala instead of Cys at postition 362. The Raman spectra show, nevertheless, that the Cys 362 sulfhydryl has a distinctly different environment in each of the three shell assemblies and thus serves as a sensitive indicator of the assembly state.

ACKNOWLEDGMENT

We thank Drs. W. R. Wikoff, Washington University, St. Louis, MO, and J. E. Johnson, Scripps Research Institute, La Jolla, CA, for providing a crystal of HK97.

REFERENCES

1. Hendrix, R. W., and Duda, R. L. (1998) Bacteriophage HK97 head assembly: a protein ballet. *Adv. Virus Res. 50A*, 235−288.

2. Conway, J. F., Duda, R. L., Cheng, N., Hendrix, R. W., and Steven, A. C. (1995) Proteolytic and conformational control of virus capsid maturation: the bacteriophage HK97 system. *J. Mol. Biol. 253*, 86−99.
3. Prevelige, P. E., Jr., and King, J. (1993) Assembly of bacteriophage P22: a model for ds-DNA virus assembly. *Prog. Med. Virol. 40*, 206−221.
4. Tuma, R., Prevelige, P. E., Jr., and Thomas, G. J., Jr. (1996) Structural transitions in the scaffolding and coat proteins of P22 virus during assembly and disassembly. *Biochemistry 35*, 4619−4627.
5. Tuma, R., Parker, M. H., Weigele, P., Sampson, L., Sun, Y., Rama Krishna, N., Casjens, S. R., Thomas, G. J., Jr., and Prevelige, P. E., Jr. (1998) A helical coat protein recognition domain of the bacteriophage P22 scaffolding protein. *J. Mol. Biol. 281*, 81−94.
6. Zhang, Z., Greene, B., Thuman-Commike, P. A., Jakana, J., Prevelige, P. E., Jr., King, J., and Chiu, W. (2000) Visualization of the maturation transition in bacteriophage P22 by electron cryomicroscopy. *J. Mol. Biol. 297*, 615−626.
7. Parker, M. H., Brouillette, C. G., and Prevelige, P. E., Jr. (2001) Kinetic and calorimetric evidence for two distinct scaffolding protein binding populations within the bacteriophage P22 procapsid. *Biochemistry 40*, 8962−8970.
8. Morais, M. C., Kanamaru, S., Badasso, M. O., Koti, J. S., Owen, B. A., McMurray, C. T., Anderson, D. L., and Rossmann, M. G. (2003) Bacteriophage φ29 scaffolding protein gp7 before and after prohead assembly. *Nat. Struct. Biol. 10*, 572−576.
9. Casjens, S., and Hendrix, R. (1988) Control mechanisms in dsDNA bacteriophage assembly in *The Bacteriophages* (Calendar, R., Ed.) pp 15−91, Plenum Press, New York.
10. Wikoff, W. R., Liljas, L., Duda, R. L., Tsuruta, H., Hendrix, R. W., and Johnson, J. E. (2000) Topologically linked protein rings in the bacteriophage HK97 capsid. *Science 289*, 2129−2133.
11. Conway, J. F., Wikoff, W. R., Cheng, N., Duda, R. L., Hendrix, R. W., Johnson, J. E., and Steven, A. C. (2001) Virus maturation involving large subunit rotations and local refolding. *Science 292*, 744−748.
12. Lata, R., Conway, J. F., Cheng, N., Duda, R. L., Hendrix, R. W., Wikoff, W. R., Johnson, J. E., Tsuruta, H., and Steven, A. C. (2000) Maturation dynamics of a viral capsid: visualization of transitional intermediate states. *Cell 100*, 253−263.
13. Tuma, R., and Thomas, G. J., Jr. (1997) Mechanisms of virus assembly probed by Raman spectroscopy: the icosahedral bacteriophage P22. *Biophys. Chem. 68*, 17−31.
14. Tuma, R., Prevelige, P. E., Jr., and Thomas, G. J., Jr. (1998) Mechanism of capsid maturation in a double-stranded DNA virus. *Proc. Natl. Acad. Sci. U.S.A. 95*, 9885−9890.
15. Tuma, R., Tsuruta, H., Benevides, J. M., Prevelige, P. E., Jr., and Thomas, G. J., Jr. (2001) Characterization of subunit structural changes accompanying assembly of the bacteriophage P22 procapsid. *Biochemistry 40*, 665−674.
16. Duda, R. L., Hempel, J., Michel, H., Shabanowitz, J., Hunt, D., and Hendrix, R. W. (1995) Structural transitions during bacteriophage HK97 head assembly. *J. Mol. Biol. 247*, 618−635.
17. Movileanu, L., Benevides, J. M., and Thomas, G. J., Jr. (1999) Temperature dependence of the Raman spectrum of DNA. I. Raman signatures of premelting and melting transitions of poly(dA-dT)·poly(dA-dT). *J. Raman Spectrosc. 30*, 637−649.
18. Benevides, J. M., Wang, A. H. J., van der Marel, G. A., van Boom, J. H., Rich, A., and Thomas, G. J., Jr. (1984) The Raman spectra of left-handed DNA oligomers incorporating AT base pairs. *Nucleic Acids Res. 12*, 5913−5925.
19. Yu, T. J., Lippert, J. L., and Peticolas, W. L. (1973) Laser Raman studies of conformational variations of poly-L-lysine. *Biopolymers 12*, 2161−2175.
20. Chen, M. C., and Lord, R. C. (1974) Laser-excited Raman spectroscopy of biomolecules. VI. Some polypeptides as conformational models. *J. Am. Chem. Soc. 96*, 4750−4752.
21. Bandekar, J. (1992) Amide modes and protein conformation. *Biochim. Biophys. Acta 1120*, 123−143.
22. Miura, T., and Thomas, G. J., Jr. (1995) Raman Spectroscopy of Proteins and Their Assemblies in *Subcellular Biochemistry* (Biswas, B. B. and Roy, S., Eds.) Vol. 24, pp 55−99, Plenum Press, New York.
23. Krimm, S. (1987) Peptides and proteins in *Biological Applications of Raman Spectroscopy* (Spiro, T. G., Ed.) pp 1−45, Wiley, New York.
24. Benevides, J. M., Weiss, M. A., and Thomas, G. J., Jr. (1991) Design of the helix-turn-helix motif: nonlocal effects of quaternary structure in DNA recognition investigated by laser Raman spectroscopy. *Biochemistry 30*, 4381−4388.
25. Berjot, M., Marx, J., and Alix, A. J. P. (1987) Determination of the secondary structure of proteins from the Raman amide I band: the reference intensity profiles method. *J. Raman Spectrosc. 18*, 289−300.
26. Overman, S. A., and Thomas, G. J., Jr. (1995) Raman spectroscopy of the filamentous virus Ff (fd, fl, M13): structural interpretation for coat protein aromatics. *Biochemistry 34*, 5440−5451.
27. Siamwiza, M. N., Lord, R. C., Chen, M. C., Takamatsu, T., Harada, I., Matsuura, H., and Shimanouchi, T. (1975) Interpretation of the doublet at 850 and 830 cm^{-1} in the Raman spectra of tyrosyl residues in proteins and certain model compounds. *Biochemistry 14*, 4870−4876.
28. Arp, Z., Autrey, D., Laane, J., Overman, S. A., and Thomas, G. J., Jr. (2001) Tyrosine Raman signatures of the filamentous virus Ff are diagnostic of non-hydrogen-bonded phenoxyls: demonstration by Raman and infrared spectroscopy of *p*-cresol vapor. *Biochemistry 40*, 2522−2529.
29. Takeuchi, H., and Harada, H. (1986) Normal coordinate analysis of the indole ring. *Spectrochim. Acta 42A*, 1069−1078.
30. Harada, I., Miura, T., and Takeuchi, H. (1986) Origin of the doublet at 1360 and 1340 cm^{-1} in the Raman spectra of tryptophan and related compounds. *Spectrochim. Acta 42A*, 307−312.
31. Miura, T., Takeuchi, H., and Harada, I. (1989) Tryptophan Raman bands sensitive to hydrogen bonding and side-chain conformation. *J. Raman Spectrosc. 20*, 667−671.
32. Takeuchi, H. (2003) Raman structural markers of tryptophan and histidine side chains in proteins. *Biopolymers 72*, 305−317.
33. Li, H., and Thomas, G. J., Jr. (1991) Cysteine conformation and sulfhydryl interactions in proteins and viruses. I. Correlation of the Raman S−H band with hydrogen bonding and intramolecular geometry in model compounds. *J. Am. Chem. Soc. 113*, 456−462.
34. Raso, S. W., Clark, P. L., Haase-Pettingell, C., King, J., and Thomas, G. J., Jr. (2001) Distinct cysteine sulfhydryl environments detected by analysis of Raman S−H markers of Cys → Ser mutant proteins. *J. Mol. Biol. 307*, 899−911.
35. Tuma, R., and Thomas, G. J., Jr. (1996) Theory, design and characterization of a microdialysis flow cell for Raman spectroscopy. *Biophys. J. 71*, 3454−3466.
36. Overman, S. A., and Thomas, G. J., Jr. (1999) Raman markers of nonaromatic side chains in an α-helix assembly: Ala, Asp, Glu, Gly, Ile, Leu, Lys, Ser, and Val residues of phage *fd* subunits. *Biochemistry 38*, 4018−4027.
37. Prevelige, P. E., Jr., Thomas, D., King, J., Towse, S. A., and Thomas, G. J., Jr. (1993) Subunit conformational changes accompanying bacteriophage P22 capsid maturation. *Biochemistry 32*, 537−543.
38. Tuma, R., Bamford, J. K. H., Bamford, D. H., Russell, M. P., and Thomas, G. J., Jr. (1996) Structure, interactions and dynamics of PRD1 Virus. I. Coupling of subunit folding and capsid assembly. *J. Mol. Biol. 257*, 87−101.
39. Tuma, R., and Thomas, G. J., Jr. (2002) Raman spectroscopy of viruses in *Handbook of Vibrational Spectroscopy* (Chalmers, J. M. and Griffiths, P. R., Eds.) Vol. 5, pp 3519−353517, John Wiley & Sons, Chichester, U.K.
40. Prevelige, P. E., Jr., Thomas, D., King, J., Towse, S. A., and Thomas, G. J., Jr. (1990) Conformational states of the bacteriophage P22 capsid subunit in relation to self-assembly. *Biochemistry 29*, 5626−5633.
41. Duda, R. L., Martincic, K., and Hendrix, R. W. (1995) Genetic basis of bacteriophage HK97 prohead assembly. *J. Mol. Biol. 247*, 636−647.
42. Gilakjan, Z. A., and Kropinski, A. M. (1999) Cloning and analysis of the capsid morphogenesis genes of *Pseudomonas aeruginosa* bacteriophage D3: another example of protein chain mail? *J. Bacteriol. 181*, 7221−7227.

BI0302494